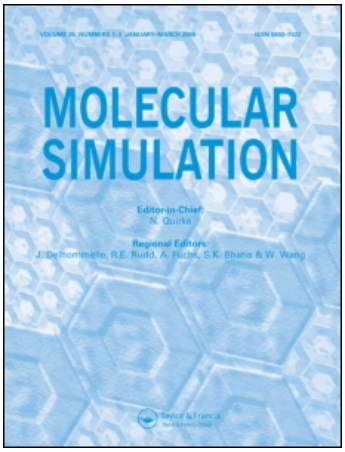

Molecular Simulation
Publication details, including instructions for authors and subscription information:
http://www.informaworld.com/smpp/title~content=t713644482

Interaction among the twelve-residue segment of antifreeze protein type I, or its mutants, water and a hexagonal ice crystal

Takashi Nobekawa[a]; Yoshimichi Hagiwara[a]
[a] Department of Mechanical and System Engineering, Graduate School of Science and Technology, Kyoto Institute of Technology, Kyoto, Japan

To cite this Article Nobekawa, Takashi and Hagiwara, Yoshimichi(2008) 'Interaction among the twelve-residue segment of antifreeze protein type I, or its mutants, water and a hexagonal ice crystal', Molecular Simulation, 34: 6, 591 — 610
To link to this Article: DOI: 10.1080/08927020801986556
URL: http://dx.doi.org/10.1080/08927020801986556

Molecular Simulation
Vol. 34, No. 6, May 2008, 591–610

Taylor & Francis
Taylor & Francis Group

Interaction among the twelve-residue segment of antifreeze protein type I, or its mutants, water and a hexagonal ice crystal

Takashi Nobekawa[1] and Yoshimichi Hagiwara*

Department of Mechanical and System Engineering, Graduate School of Science and Technology, Kyoto Institute of Technology, Matsugasaki, Kyoto, Japan

(*Received 23 April 2007; final version received 12 February 2008*)

We have carried out a molecular dynamics analysis on a mixture of supercooled water, a hexagonal ice crystal and segments of winter flounder antifreeze protein. The segment consists of nine alanine residues, two threonine residues and one asparagine residue. Mutant segments, in which the threonine residues are replaced with valine residues, or serine residues, are also used. It is found that the threonine residue near the asparagine residue of the original segment is located in the vicinity of the prism face of the ice crystal. This is due to the hydrogen bond between the hydrophilic sites of these residues and water molecules, and the hydrogen bond between these water molecules and the water molecules on the ice surface. The valine and serine residues in the mutant segments do not approach the prism face of the ice crystal compared with the threonine residue near the asparagine residue. The motion of five segments, closely located side by side, is not remarkable. This is because of the gathering of water molecules caused by hydrophobic hydration, not only around alanine residues but also around the methyl sites of threonine residues.

Keywords: antifreeze protein type I; segments; mutant segments; angular distribution function; hexagonal ice crystal

1. Introduction

Attention has recently been paid to the inhibition of ice crystal growth. This inhibition is important for improving the taste of frozen foods, according to Li and Sun [1]. It is also important for the development of freeze-resistant fish in aquaculture, and the production of cold-hardy plants in agriculture (see Fletcher et al. [2]). Furthermore, it is necessary for preserving organs which are to be transplanted, according to Amir et al. [3].

One of the most promising methods for the inhibition is the use of an additive, which has the function of lowering the freezing point while retaining the melting point. The growth of ice can be controlled easily by keeping the preservation temperature in the range between the two points. Antifreeze proteins (AFPs) are appropriate additives because they cause a wide gap between the two points, and are non-toxic. Furthermore, they do not increase osmotic pressure. These characteristics of AFPs are superior to those of sodium chloride and a disaccharide.

Among various AFPs, HPLC6 has been focused on in many experiments and molecular dynamics studies. The HPLC6 is the major fraction of winter flounder antifreeze protein. Yang et al. [4] clarified from the analysis of the X-ray crystallographic structure of HPLC6, that the HPLC6 consists of 37 residues of amino acids and forms α-helix. More than two thirds of these residues are hydrophobic alanine residues. Four hydrophilic threonine residues are positioned on one side of the helix at nearly identical distances. Thus, the following hypothesis has been accepted: the hydrogen atoms of the hydroxyl sites of the threonine residues are bonded to the oxygen atoms on the pyramidal plane of $(20\bar{2}1)$ in the ice *Ih* crystal, because the distance of the hydrogen atoms is nearly equal to the repetitive distance of the oxygen atoms along the direction of $(10\bar{1}2)$ on the plane (see Knight et al. [5]). Consequently, many alanine residues orient themselves toward the opposite direction from the ice surface. Thus, the residues interfere with the approach of water molecules to the ice surface (see, for example, Ye and Feeney [6]). This is consistent with the fact obtained by Chao et al. [7] and Zhang and Laursen [8] that only bi-pyramidal ice crystals were observed in the solution of the HPLC6 below the freezing point of water.

However, experimental results inconsistent with these hypotheses have been obtained recently by using mutants of HPLC6. Table 1 shows typical mutants dealt with by Chao et al. [7], Zhang and Laursen [8], Haymet et al. [9] and Loewen et al. [10]. The ratio of the thermal hysteresis of each mutant in the case of its concentration of 5 mg/ml to that of HPLC6 is also indicated in the table. In addition, the growth of an ice crystal, whose shape is hexagonal bipyramid or trapezohedron, is summarised

*Corresponding author. Email: yoshi@kit.ac.jp

ISSN 0892-7022 print/ISSN 1029-0435 online

DOI: 10.1080/08927020801986556
http://www.informaworld.com

Table 1. Comparison of mutants of HPLC6.

	Residues of mutants						Ratio of thermal hystereses	Ice growth
HPLC6	Thr2	Thr13	Asn16	Thr24	Asn26	Thr35	1	No
Chao [7]	Thr	**Val**	Asn	**Val**	Asn	Thr	0.86	No
Zhang [8]	**Val**	**Val**	Asn	**Val**	Asn	**Val**	0.33	Gradual
Haymet [9]	**Val**	**Val**	Asn	**Val**	Asn	**Val**	0.85	No
Chao [7]	Thr	Ser	Asn	**Ser**	Asn	Thr	0.14	Yes
Zhang [8]	Thr	Ser	Asn	Thr	Asn	Thr	0.90	No
	Thr	Thr	Asn	**Ser**	Asn	Thr	0.72	No
	Ser	Thr	Asn	Thr	Asn	**Ser**	0.68	No
	Ser	Thr	Asn	**Ser**	Asn	**Ser**	0	Yes
	Ser	**Ser**	Asn	**Ser**	Asn	**Ser**	0	Yes
Loewen [10]	Thr	Thr	**Thr**	Thr	**Thr**	Thr	1.09	No
	Thr	Thr	**Val**	Thr	**Val**	Thr	0.63	No
	Thr	Thr	**Gln**	Thr	**Gln**	Thr	0	–

in the table. It is found from the table that the hydroxyl groups and methyl groups in the threonine residues can contribute to the antifreeze activity, as Zhang and Laursen [8] and Jorov et al. [11] pointed out. Furthermore, the atom groups in the asparagine residue (Asn27) also contribute to the antifreeze activity.

In order to investigate the roles of residues in more detail, many molecular dynamics studies have been carried out. Cheng and Merz [12] noted that both the hydrogen bond and van der Waals' interaction play an important role in the binding of protein onto the ice surface. They also mentioned that hydrophobic interactions might be important. Dalal et al. [13] investigated the effect of the HPLC6 molecule on the water molecules in the liquid phase near the pyramidal face of the ice crystal. They concluded that there is no gain in hydrogen bonds when interaction occurs between the proteins and the ice/water interface. Wierzbicki et al. [14] carried out a molecular dynamics simulation of liquid water with two models of the HPLC6 along an ice plate covered with the pyramidal planes of $(20\bar{2}1)$. They obtained results supporting the hypothesis that the hydrophobic side of the protein model is oriented toward the pyramidal plane. Yang and Sharp [15] found that the mutant, in which the threonine residues were replaced with hydrophilic serine residue, caused a polar-like hydration. Nevertheless, the interactions between water molecules and the sites of amino acid residues in the HPLC6, or in its mutant, have not yet been clarified.

The present authors consider that the aforementioned molecular dynamics analyses predict the latter stage of the whole antifreeze activity of HPLC6. On the other hand, the early stage of the whole activity, when the HPLC6 is located close to an ice surface, has not yet been clarified. This early stage may occur in the blood flow in the capillary of winter flounder. In this case, quite low heat flux exists, and thus, the thermal state is not in equilibrium. These thermal conditions are not the same as those in the crystal growth tests carried out by Chao et al. [7], Zhang and Laursen [8], Haymet et al. [9] and Loewen et al. [10], but similar to those in the crystal habit tests (or the one-dimensional ice growth tests in a narrow gap) carried out by Haymet et al. [16] and Coger et al. [17]. When the concentration of AFP and the growth rate of ice (and thus heat flux) are low, only prism faces are observed in the crystal habit test conducted by Coger et al. [17]. When the concentration of AFP and the growth rate of ice are high, not only prism faces but also pyramidal planes (though not necessarily the pyramidal plane of $(20\bar{2}1)$) are observed.

The images of ice surfaces obtained by Haymet et al. [16] and Coger et al. [17] suggest that the pyramidal planes are formed from the edge of the prism faces. Therefore, it is worth analysing the interactions among the prism faces of ice, HPLC6 and surrounding water in order to elucidate the formation mechanism of bipyramidal ice crystals.

The concentration of AFP near the interface increases as an ice crystal grows because of the solute displacement through the solidification process. If the local concentration of AFP is high, diffusion of AFP due to the concentration gradient and the aggregation of AFP can occur. The present authors consider that the diffusion and aggregation are also key factors of the antifreeze activity. These factors are taken into account in the studies on many other biopolymers. The diffusion and aggregation of AFP may attenuate the adsorptions of water and itself to the ice surfaces. Furthermore, the diffusing or aggregating AFP may affect and swing the adsorbed water molecules, or AFP, on the ice surface. However, as far as the present authors know, diffusion and aggregation of HPLC6 have not yet been discussed in detail.

We have carried out molecular dynamics analyses of water with an ice nucleus and the model of part of the HPLC6. The goal of our study is to elucidate the early

stage of the interaction between the HPLC6 and a growing ice nucleus, which may appear in winter flounder. In our previous paper (Nobekawa et al. [18]), we have investigated the interaction between water molecules and the sites of a segment of HPLC6 or its mutants. The threonine residues in the original segment were replaced with valine residues, or serine residues, in the mutant segments. In the present study, we focus on the interaction between the sites of residues in the segments and the water molecules close to the prism faces of the ice crystal. The effects of the five segments on the water molecules near the faces of the ice crystal are also discussed.

2. Simulation procedures

The following procedures are the same as those in our previous paper [18] except for the procedures in Sections 2.4 and 2.6.3.

2.1 Assumptions

The number of molecules, the volume of the computational domain and the total energy were kept constant except for the period of the temperature scaling mentioned below. Strictly speaking, in the solidification process, the temperature is unchanged but the total energy changes. However, the computation period in the present study was very short, as shown below. Thus, we considered that the assumption is reasonable. All the water molecules were assumed to be rigid bodies. The periodic boundary condition was imposed on the computational domain.

2.2 Governing equations

The Newton–Euler equations for the translational and rotational motions of the molecules were solved at each time step, and were integrated with time by using the Gear algorithm [19]. We used a 5-value Gear algorithm, in which the time derivatives up to the fifth order were considered, to the Newton equation for the translational motion. We adopted a 4-value Gear algorithm to the Euler equation for the rotation. All the computations were carried out with the time steps of 0.5 fs.

2.3 Temperature scaling

The statistical temperature, T, was given by the total energy of the translational motion for all the molecules, K_T, and that of the rotational motion for the molecules, K_R. The temperature is written as follows:

$$T = \frac{1}{2}\left(\frac{2}{3k_B N}K_T + \frac{2}{3k_B N}K_R\right) = \frac{1}{3k_B N}\left(\frac{1}{2}\sum_{i=1}^{N}\left(mv_{xi}^2 + mv_{yi}^2 + mv_{zi}^2\right) + \frac{1}{2}\sum_{i=1}^{N}\left(I_{px_i}\omega_{px_i}^{\ 2} + I_{py_i}\omega_{py_i}^{\ 2} + I_{pz_i}\omega_{pz_i}^{\ 2}\right)\right) \quad (1)$$

where k_B is the Boltzmann constant, N is the total number of molecules, m is the mass of molecules, and I_p is the inertia moment based on its principal axis. Temperature scaling was carried out, in which the translational velocity, $\boldsymbol{v}$, and the angular velocity, $\boldsymbol{\omega}$, of each molecule were changed by the following equation:

$$\boldsymbol{v}_i^{(\mathrm{new})} = \boldsymbol{v}_i^{(\mathrm{old})}\sqrt{\frac{T_{\mathrm{pd}}}{T}}, \quad \boldsymbol{\omega}_i^{(\mathrm{new})} = \boldsymbol{\omega}_i^{(\mathrm{old})}\sqrt{\frac{T_{\mathrm{pd}}}{T}}, \quad (2)$$

where T_{pd} is the predetermined temperature.

2.4 Production of ice–water mixture

We adopted a small computation domain including a small ice crystal (Case A), and a large computation domain including a large ice crystal (Case B). We produced the ice–water mixture by using the following six-stage procedure.

Stage 1. A small ice cube with *Ih* structure is formed. This procedure is the same as that described in our previous study (Iwasaki and Hagiwara [20]). A total of 360 water molecules are in a cubic domain of approximately 2.25 nm. In this domain, the centre of mass of each molecule is allocated at the lattice of *Ih* structure. The orientation of hydrogen atoms is randomly determined. Then, eight ice cubes are connected to each other so that the dimensions of the new ice cube are double the original. This ice cube is used for Case A. Similarly, 27 ice cubes are connected to each other so that the dimensions of the new ice cube are triple the original. This ice cube is used for Case B. The dimensions of these new ice cubes and hence, the dimensions of computation domains are shown in Table 2.

Stage 2. A stabilisation procedure is carried out for water molecules in the ice cubes. In this procedure, the temperature of the ice cubes is decreased step by step to 240 K. During the procedure, the restraint condition is used for the displacement of water molecules, which is illustrated in Table 3. Note that the origin of time is set at the instant when the segments are introduced. The statistical quantities are calculated for the motion of water molecules for the final period of 25 ps in the stabilisation.

Stage 3. 378 (Case A) or 1254 (Case B) water molecules in a hexagonal-prism region are specified as the molecules forming the ice crystal (see Table 2). The a_1-axis

Table 2. Computational condition.

	Case A	Case B
Number of molecules in ice	378	1254
Number of molecules in water	2413	8274(8275)[a]
Computational domain (nm)	4.667 × 4.491 × 4.400	7.000 × 6.736 × 6.600
Prism face area (nm^2)	1.04 × 3.03	1.81 × 3.76
Density (g/cm^3)	0.906	0.916
α	5.6	12.4

[a] In the case with VV segment

Table 3. Stabilisation of water molecules in ice cubes.

		Period (ps)	
Motion of water molecules of ice	Temperature (K)	Case A	Case B
Fixed	265	−400 to −375	−550 to −525
0.01%[a]	265	−375 to −350	−525 to −500
0.10%	265	−350 to −325	−500 to −475
1%	265	−325 to −300	−475 to −450
10%	265	−300 to −275	−450 to −425
30%	255	−275 to −250	−425 to −400
50%	250	−250 to −225	−400 to −375
60%	245	−225 to −200	−375 to −350
Free	240	−200 to −175	−350 to −325
Free	Free	−175 to −150	−325 to −300

[a] The displacement was reduced to 0.01% of its predicted value.

of the ice crystal is positioned parallel to the *x*-axis of the Cartesian coordinate system, and the *c*-axis of the crystal is positioned parallel to the *z*-axis of the Cartesian coordinate system. The area of each prism face is shown in Table 2. The area is wider than the segment, so the interactions among the water molecules in the liquid phase, the water molecules in the ice crystals and the segments can be predicted. Since, the ice crystal occupies only 13% of the whole domain, the minimum distance between the edge of the ice crystal and that in the mirror image is longer than half of the side of the domain in both cases. Therefore, the ice crystal has the advantage in that the motion of the molecules is not affected noticeably by the mirror images of the ice crystal.

Stage 4. The ice outside the hexagonal-prism region is melted. To achieve this, the temperature scaling is applied to the translational and rotational velocities of each molecule except for the molecules in the ice crystal region. The predetermined temperature is 330 K (see Table 4). The coordinates and other physical values of the molecules in the ice crystal region are not updated through the scaling procedure. This procedure corresponds to the energy input. We confirmed whether the molecules are in a liquid phase or a solid phase by using the mean square displacement (MSD) and the radial distribution function (RDF).

Stage 5. The water in the liquid phase is cooled in order to obtain the supercooled water. The temperature scaling is carried out for the translational and rotational velocities of each molecule except for the molecules in the ice crystal region. The predetermined temperature is set at 300 K and then lowered to 230 K (see Table 4). The coordinates and other physical values for the molecules in the ice crystal region are not updated through the scaling procedure. The water outside the ice crystal region is confirmed not to be in the amorphous state by using the MSD of water molecules.

Table 4. Procedure of making the ice–water mixture.

			Period (ps)	
Motion of water molecules in ice	Motion of water molecules in liquid phase	Temperature of liquid phase (K)	Case A	Case B
Fixed	Free	330	−150 to −100	−300 to −270
Fixed	Free	300	−100 to −90	−270 to −240
Fixed	Free	230	−90 to −80	−240 to −210
Fixed	Free	Free	−80 to −70	−210 to −180
Free	Free	Free	−70 to −50	−180 to −150

Stage 6. The restraint of the water molecules in the ice crystal region is removed. Then, the computation is carried out for a relaxation period in which the coordinates of all the molecules were updated. The mixture of water and ice crystal is confirmed to be established by using the MSD of water molecules. The result thus obtained by the preliminary computation is used as the database in order to introduce the segments mentioned below.

2.5 Potential functions of water molecules

The TIP4P potential proposed by Jorgensen et al. [21] was used for the potential function for the interaction between two water molecules. This potential was developed for water in a liquid phase. Nevertheless, ice/water mixture with proteins and water solidification (see Matsumoto et al. [22]) can be predicted using this potential. Recently, a reasonable potential was newly proposed by Nada et al. [23]. However, we did not adopt this new potential in this study, partly because the ice growth rate was too high in their result and partly because the interaction between the water molecule and the sites of amino acid residues in proteins has not yet been investigated using the new potential.

The TIP4P potential consists of the Coulomb potential and the Lennard-Jones potential. In order to reduce the effect of far distant molecules, a cutoff radius was set for the Lennard-Jones potential. Since we applied the group-based cutoff to the procedure, the cutoff radius of the atom group was measured from the indicator point of the group. The point was allocated at its centre of mass for each water molecule. In addition, we did not adopt the method of a non-bonded neighbour list proposed by Verlet [24] in this paper, because the prism faces of the ice crystals are not so wide and thus the number of water molecules on the faces is not high enough. The Ewald method (see Frenkel and Smit [25]) was used for the Coulomb potential in order to reduce the electrical force of far distant molecules. The parameters for the Ewald summation were $\alpha = 5.6$ in Case A or 12.4 in Case B (see Table 2), $|\mathbf{u}|_{\max} = 1$ and $|\mathbf{h}|^2_{\max} = 27$ where α is the width of the Gaussian distribution, $\mathbf{u}$ is the vector for the location of the image cell in the physical space and $\mathbf{h}$ is the vector for the location of the image cell in the Fourier space.

The net dipole was not evaluated for the following reasons: if the sum of the electrical charge is not constant for the atoms inside the spherical region, whose radius is the cutoff radius, corrections of the electrical charges are necessary for the atoms outside the region at each time step. This is because of the periodic boundary condition in the three directions for the computational domain of limited size. These corrections cause a difficulty in the calculation. Furthermore, as far as the present authors know, there is no discussion about the specific dipole, which is available for the gradual solidification or melting of water molecules at the ice/water interface. Thus, we assigned zero electrical charge, for simplicity.

2.6 Segment of HPLC6

2.6.1 Conformation

The segments are the same as those adopted in our previous paper (Nobekawa et al. [18]). Figure 1(a) shows the original segment (TT segment). This segment consists of 12 amino acid residues, namely Thr24, Ala25, Ala26, Asn27, Ala28, Ala29, Ala30, Ala31, Ala32, Ala33, Ala34 and Thr35. Although, the segment has the disadvantage in that the effect of other amino acid residues of the HPLC6 on the segment cannot be considered, it has the advantages in that the effect of hydrophilic residues can be highlighted and the segment is small enough to obtain reliable statistics concerning the interaction between the segment and surrounding water molecules. Each methyl site is replaced with a single imaginary atom for simplicity. The atom group of CO—NH—CH_3 is connected to the other side of the alanine residue of each threonine residue in order to reduce the terminus effect on the threonine residues. The atoms in these groups are surrounded with broken lines in the figure. Hereafter, the hydrogen site far from the helical axis in the amino group of Asn27 is designated as H_{N1}, and the other hydrogen site is designated as H_{N2}, in order to discuss the hydrogen bond between these hydrogen sites and the oxygen atoms of water molecules.

Figure 1(b) indicates the TT segment viewed along the α-helical axis. In the α-helical conformation, 3.6 residues exist per turn and the pitch of turn (i.e. the distance of the helix rises along its axis per turn) is 0.54 nm. In order to make the discussion clear, we divide the segment into two sides: the hydrophobic side, in which only the alanine residues (Ala25, Ala26, Ala29, Ala30, Ala32 and Ala33) are included, and the hydrophilic side, in which the other residues (Thr24, Asn27, Ala28, Ala31, Ala34 and Thr35) are included. This classification is different from the three-face classification proposed by Jorov et al. [11]. This is because our segment does not contain the four residues (Ser4, Lvs18, Glu22 and Arg37), which form the boundary between the hydrophobic side and hydrophilic side in their classification.

The dihedral angles of the peptide bond, φ and ψ, were retained at −57 and 48°, respectively, which are based on the angles of an ideal α-helix described by Cheng and Merz [12]. Thus, the segment conformation was unchanged through the computation. This rigidness can be considered as an overestimation of the hydrogen bond between two adjacent sites in the axial direction of the segments. Flexibility can be considered by adopting an algorithm, such as SHAKE, developed by Ryckert et al. [26]. However, we did not include any algorithm for the flexibility because the time constants of the

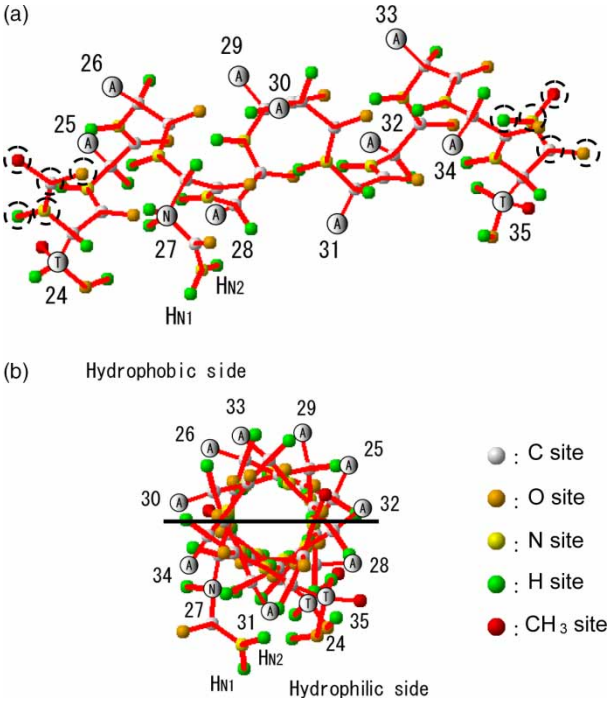

Figure 1. TT segment: (a) view from side, (b) view from the helical axis.

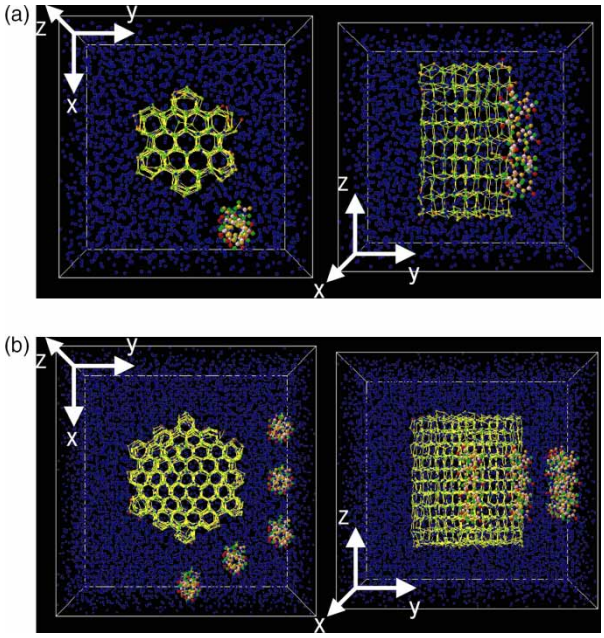

Figure 2. Locations of oxygen atoms of water molecules and sites of segments in the initial condition of computation: (a) Case A (small domain), (b) Case B (large domain).

deformation of AFPs are not clear. In addition, the dihedral angles of the central residues of HPLC6 fluctuated within 9°, in the molecular dynamics simulation with Assisted Model Building with Energy Refinement (AMBER), according to Cheng and Merz [12]. Therefore, the rigid segments are not too unrealistic. The dihedral angles of sites of the atom group in the residues were also determined from the angles in the table illustrated by Cheng and Merz [12].

We made one mutant segment (VV segment) from the TT segment by replacing the hydroxyl group in the two threonine residues with the methyl site. Similarly, we made another mutant segment (SS segment) from the TT segment by replacing the methyl site in the threonine residues with the hydrogen atom.

2.6.2 *Potential functions*

The Optimized Potentials for Liquid Simulations (OPLS) parameters developed by Jorgensen et al. [27] were adopted as the potential parameters of each site of the segment. The electric charge was defined at the methyl site in one end (i.e. the C-terminus connected to Thr24, Val24 or Ser24) so that the sums of the electric charge of the segments were zero. The cutoff radius was 1.5 nm. The centre of the radius was set at the indicator point of each group of sites. The point was allocated at the centre of the group where the electric charge was zero (see Reach [28]). The parameters for the Ewald summation of the water–water interaction were used for the parameters for the summation of the water-site interaction.

Table 5. Stabilisation for the mixture of water, an ice crystal and segments.

Motion of segments	Motion of water molecules in ice	Motion of water molecules in liquid phase	Temperature (K)	Period (ps) Case A	Period (ps) Case B
Fixed	Fixed	Free	230	–	−150 to −120
0.010%[a]	Fixed	Free	230	−50 to −40	−120 to −90
Free	Fixed	Free	230	−40 to −30	−90 to −60
Free	Free	Free	230	−30 to −20	–
Free	Fixed	Free	Free	–	−60 to −30
Free	Free	Free	Free	−20 to 0	−30 to 0

[a] The displacement was reduced to 0.10% of its predicted value.

2.6.3 Introduction of segments into ice–water mixture

Some water molecules were removed from cocoon-shaped regions in the database mentioned in 2.4. The longest axes of these regions and thus the axes of the segments, were parallel to the z-axis. In Case A, one segment was introduced into one vacancy near the $(10\bar{1}0)$ prism face of the ice crystal. The hydrophobic side of the segment faced towards the positive direction on the x-axis. In Case B, five segments were introduced into five vacancies near the $(10\bar{1}0)$ and $(01\bar{1}0)$ prism faces of the ice crystal. The hydrophobic sides of all the segments faced towards the positive direction on the x-axis. The distance between the axes of two neighbouring segments was equal to 1.55 nm. This distance was determined from the molecular simulation result obtained by Nguyen et al. [29], in which the potential energy of two parallel AFP molecules took the minimum value.

The scaling of velocity was carried out immediately after the introduction of the segments into the domain. The scaling procedure is summarised in Table 5. This procedure is the same as that explained in our previous study (Nobekawa et al. [18]). The coordinates and other physical values of the molecules in the ice crystal region were not updated through the scaling procedure except for the final short period. In this final period, all the restraints were removed. Consequently, we obtained the initial condition of the main computation. Figure 2(a) and (b) demonstrate the locations of oxygen atoms of water molecules and sites of segments in the initial condition in Case A, and those in the initial condition in Case B, respectively. The dots indicate the location of the atom and sites. The yellow lines in the figure depict the hydrogen bonds between water molecules in the ice crystal.

3. Statistical quantities

After finishing the stabilisation procedure for the mixture of water, an ice crystal and segments mentioned above, the computations were carried out for the periods of 0–250 ps, in Case A and 0–1 ns, in Case B, in order to obtain statistical quantities. The time series of orientation and displacement of segments were monitored through these periods. The potential energy was also monitored in the periods. The following six functions were obtained. These functions are the same as those defined in the first report (Nobekawa et al. [18]) except for the final function defined in 3.6.

3.1 Mean square displacement

The MSD of water molecules, $D(t)$, is defined by the following equation:

$$D(t) = \frac{1}{N}\left\langle \sum_j \left|\mathbf{r}_j(t_0 + t) - \mathbf{r}_j(t_0)\right|^2 \right\rangle, \qquad (3)$$

where $\mathbf{r}_j$ is the position vector of a molecular j, t is time, t_0 is a reference time, N is the number of molecules and the angle bracket shows a time mean value. The MSD was obtained from the position vectors for the periods of 10 ps at an interval of 0.25 ps. The moving-averaged values of the MSD over the period of 50 ps (i.e. 200–210, 200.25–210.25, 200.5–210.5, ..., 240–250 ps in Case A, and 350–360, 350.25–360.25, 350.5–360.5, ..., 390–400 ps in Case B) will be discussed later.

3.2 Correlation function of rotation

The rotational motions of each water molecule are investigated using the correlation function of rotation, $C_R(t)$. The correlation function (CFR) is defined by the following equation:

$$C_R(t) = \frac{1}{2N}\left\langle \sum_j \left[3\left\{\mathbf{u}_j(t_0 + t) - \mathbf{u}_j(t_0)\right\}^2 - 1\right] \right\rangle$$

$$= \frac{1}{2N}\left\langle \sum_j \left[3\cos^2\theta_j(t) - 1\right] \right\rangle \qquad (4)$$

where $\mathbf{u}_j(t_0)$ is the unit vector of one O—H axis in a molecule j at t_0, and $\theta_j(t)$ is the angle between $\boldsymbol{u}_j(t_0 + t)$ and $\boldsymbol{u}_j(t_0)$. If the rotational motion is retained, the randomness of the motion is reduced. In this case, the CFR keeps high values. The CFR was obtained from the unit vectors for the periods of 10 ps, at an interval of 0.25 ps. The moving-averaged values of the CFR over the period of 50 ps (i.e. 200–210, 200.25–210.25, 200.5–210.5, ..., 240–250 ps in Case A, and 350–360, 350.25–360.25, 350.5–360.5, ..., 390–400 ps in Case B) will be discussed later.

3.3 Radial distribution function

The RDF between an atom of water molecule or a site of the segments and the oxygen atoms in a spherical shell is defined as follows (see for example, Allen and Tildesley [30]):

$$g(r) = \frac{V}{4\pi r^2 \Delta r N^2}\left\langle \sum_i \sum_{j\neq i} \delta\left(\mathbf{r}_i - \mathbf{r}_j\right) \right\rangle, \qquad (5)$$

where $r = |\mathbf{r}_i - \mathbf{r}_j|$ is the distance between two atoms (or between a site and an atom), V is the volume of computational domain, Δr is the thickness of the shell, N is the number of oxygen atoms and δ is the delta function. Δr was equal to 0.01 nm.

3.4 Angular distribution function

Yang and Sharp [15] discussed the probability distribution of water–water angles. This distribution is effective for estimating the overall hydrogen bond between water molecules. However, it depends on the distance between two molecules, and is not sufficient for considering the hydrogen bond between an oxygen atom or a hydrogen atom in the residues of the segments and water molecules.

In our previous paper (Nobekawa et al. [18]), we introduced the angular distribution function (ADF), a new bivariate function of the angle α_{HB} and distance r. This angle is defined by the two lines as follows: the first line passes through the atom (or the site) at the shell centre and an oxygen atom inside the shell. When the oxygen atom of a water molecule is located at the shell centre as shown in Figure 3(a), the second line is along the covalent bond between the oxygen atom inside the shell and the hydrogen atom located at a farther distance than the other hydrogen atom. (Hereafter, the solid line between two atoms represents the covalent bond, and the dotted line between two atoms represents the hydrogen bond).

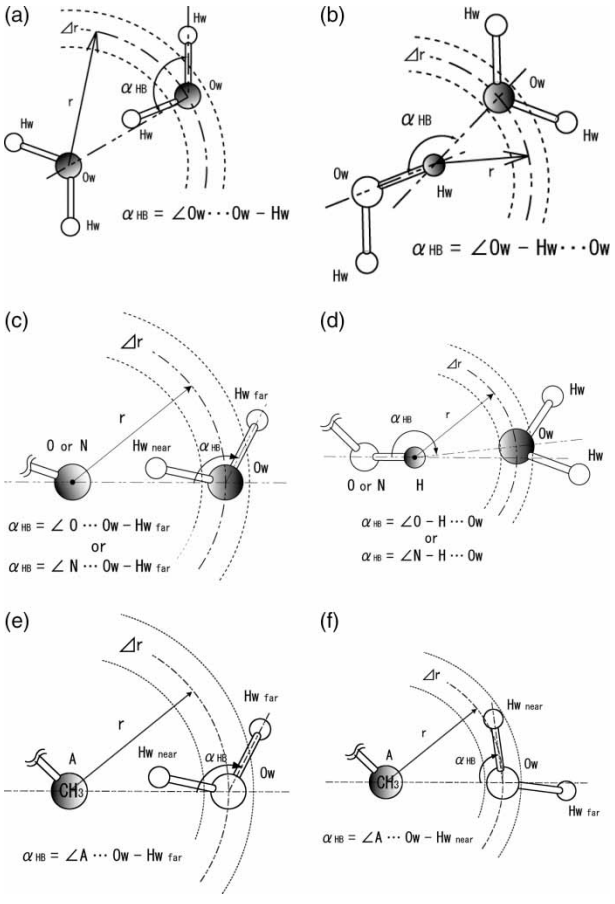

Figure 3. Angle of α_{HB} in the definition of ADF: (a) $O_w\cdots O_w$—$H_{w\,far}$, (b) O_w—$H_w\cdots O_w$, (c) O (or N)$\cdots O_w$—$H_{w\,far}$, (d) O (or N)—$H\cdots O_w$, (e) A (CH_3)$\cdots O_w$—$H_{w\,far}$ and (f) A (CH_3)$\cdots O_w$—$H_{w\,near}$.

When one of the hydrogen atoms of a water molecule is at the shell centre, as shown in Figure 3(b), the second line is along the covalent bond between the hydrogen atom at the shell centre and the oxygen atom. The angle shown in Figure 3(b) is useful for examining the hydrogen bond among several water molecules.

The definition of α_{HB} can be expanded in the case where an atom of the segments is located at the shell centre. When the oxygen site or nitrogen site of a hydrophilic group of the segments is at the shell centre as shown in Figure 3(c), the second line is along the covalent bond between the oxygen atom inside the shell and the hydrogen atom located at a farther distance than the other hydrogen atom. When a hydrogen site of a hydrophilic group of the segments is at the shell centre as shown in Figure 3(d), the second line is along the covalent bond between the hydrogen site and the oxygen site or nitrogen site of the hydrophilic group. When a methyl site of the segments is at the shell centre, the second line is along the covalent bond between the oxygen atom and the hydrogen atom located at a longer distance from the methyl site as shown in Figure 3(e). In this case, the other line is along the covalent bond between the oxygen atom and the hydrogen atom located at a shorter distance from the methyl site as shown in Figure 3(f).

The ADF is defined as follows:

$$A(r, \alpha_{HB}) = g(r)\frac{\sum n(r, \alpha_{HB})}{\sum_{\alpha_{HB}=0^\circ}^{180^\circ}\sum n(r, \alpha_{HB})}, \qquad (6)$$

where n is the number of water molecules whose oxygen atoms are located inside the spherical shell mentioned above and form an angle of α_{HB} with the atom (or the site) at the shell centre. The RDF is multiplied in order to reduce the effect of an increase in the number of water molecules with the distance on the function.

3.5 Dihedral angular distribution function

Since we replaced each methyl site with the single atom, we can specify the water molecules inside the first hydration shell of a methyl site by using the RDF of the site. Furthermore, we can examine the orientation of the specific water molecules by considering the dihedral angle β of the water molecules. Figure 4 indicates the dihedral angle defined by the three atoms of the water molecule and the methyl site. The dihedral angular distribution function (DADF) is defined as follows:

$$T(r, \alpha_{HB}, \beta) = A(r, \alpha_{HB})\frac{\sum n(r, \alpha_{HB}, \beta)}{\sum_{\beta}\sum n(r, \alpha_{HB}, \beta)}. \qquad (7)$$

The dihedral angle is equal to 0°, when the three atoms and the site are on a plane.

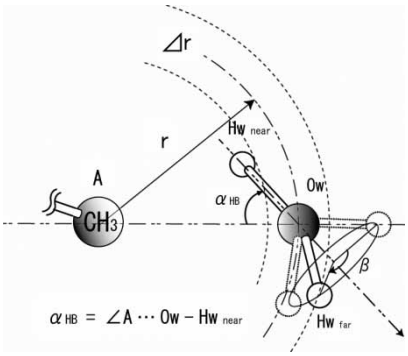

Figure 4. Dihedral angle of β in the definition of DADF.

3.6 *Hydrogen-bond correlation function*

Umemura et al. [31] proposed the hydrogen-bond correlation function (HBCF) in order to analyse the hydrogen bond in the clusters of water molecules. We modified their definition of the function and used it in order to discuss the effect of the segments on the clusters. The function is defined as follows:

$$C_{\mathrm{HB}}(t) = \frac{\left\langle \sum_j^N n_{\mathrm{HB}j}(t_0 + t)\, n_{\mathrm{HB}j}(t_0) \right\rangle}{\left\langle \sum_j^N n_{\mathrm{HB}j}(t_0)\, n_{\mathrm{HB}j}(t_0) \right\rangle}, \qquad (8)$$

where $n_{\mathrm{HB}j}(t_0)$ is the number of water molecules bonded with a molecule j at a reference time t_0, and $n_{\mathrm{HB}j}(t_0 + t)$ is the number of water molecules that have maintained the hydrogen bond with a molecule j for the period of t. The cluster structure was identified only by the distance r of water molecules from a specific water molecule ($r = 0.35$ nm) or a specific site of the segments ($r = 0.55$ nm). These values are based on the radii of the first and second hydration shells.

4. Results and discussion

4.1 *Verification of ice–water mixture*

Firstly, we examine whether or not the ice crystal formed an ice *Ih* structure just before the introduction of segments. Figure 5(a) and (b) indicate the ADF for the water molecules, which was calculated in the final 25 ps during the stabilisation procedure shown in Table 3. The highest peak is seen at $r = 0.28$ nm and $\alpha_{\mathrm{HB}} = 104°$ in Figure 5(a). These values correspond to the hydrogen bond of two adjacent water molecules. The second highest peak is located at $r = 0.44$ nm and $\alpha_{\mathrm{HB}} = 142°$. The third highest peak is located at $r = 0.44$ nm and $\alpha_{\mathrm{HB}} = 90°$. The value of $r = 0.44$ nm is equal to two oxygen atoms in the $(01\bar{1}0)$ direction on the $(2\bar{1}\bar{1}0)$ secondary prism plane of the ice *Ih* structure. One of the hydrogen atoms of these water molecules is on the prism plane, and the other hydrogen atom is out of the plane. In this case, the angle between the hydrogen atom and the oxygen atom should be 90° and 142°, respectively. These angles are in agreement with α_{HB} for the third peak and second peak, respectively. Similarly, the highest peak is seen at $r = 0.18$ nm and $\alpha_{\mathrm{HB}} = 180°$ in Figure 5(b). These values correspond to the hydrogen bond of two adjacent water molecules. The second highest peak is located at $r = 0.31$ nm and $\alpha_{\mathrm{HB}} = 56°$. The value of $r = 0.31$ nm is equal to two oxygen atoms on the $(10\bar{1}0)$ prism plane of the ice *Ih* structure. In this case, the angle between the hydrogen atom and the oxygen atom should be 59°. This angle is nearly equal to α_{HB} for the second peak. Thus, it is confirmed that the ice *Ih* structure was obtained.

We examine the state of the water molecules before introducing the segments into the computational domain. Figure 6(a) and (b) show the MSD of water molecules in Case A and that in Case B, respectively. The MSD was obtained from the position vectors for the period of 10 ps at an interval of 0.25 ps. The moving averages are

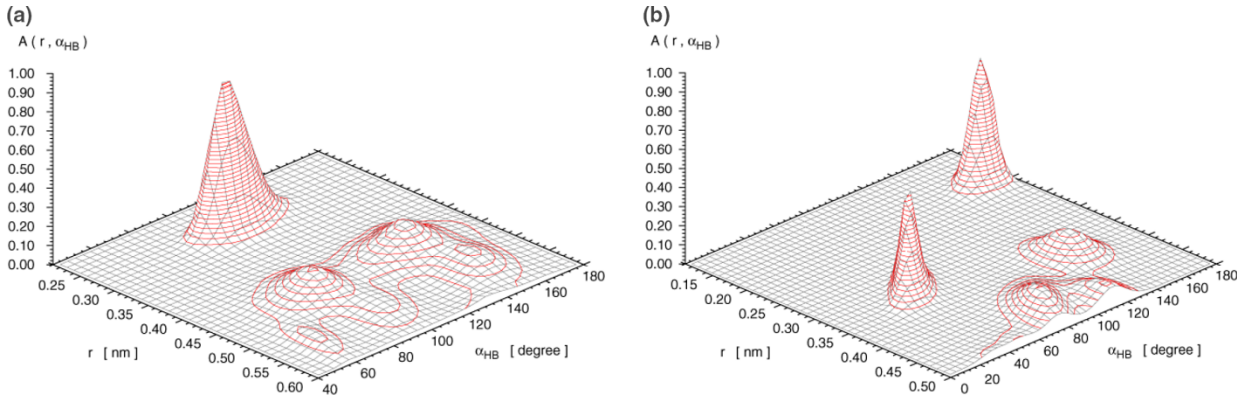

Figure 5. ADFs of water molecules in ice: (a) $O_w \cdots O_w — H_w$, (b) $O_w — H_w \cdots O_w$.

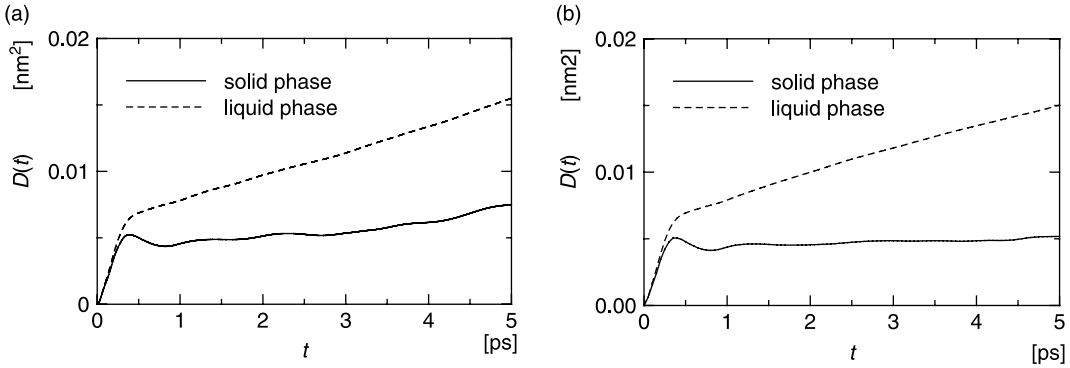

Figure 6. MSDs of water molecules: (a) Case A, (b) Case B.

calculated for the final 50-ps periods during the procedures of making the ice–water mixture: −70– − 60, −69.75– − 59.75, . . . , −60– −50 ps in Case A, and −180– − 170, −179.75– − 169.75, . . . , −160– − 150 ps in Case B. The initial instants for these moving averages are indicated as $t = 0$ ps in the figure, for simplicity. The solid lines indicate the results of the water molecules in the ice crystals, and the broken lines indicate the results of the water molecules in the liquid regions. The MSD of water molecules in the ice crystals does not increase noticeably as time proceeds. In contrast with this, the MSD of water molecules in the liquid regions increases. This shows that the water molecules in the liquid region diffuse continuously. Furthermore, it is confirmed that the potential energy of the water molecules in the ice crystals is clearly lower than that in the liquid regions (figure omitted). Thus, it is proven that the water outside the ice crystals is in a supercooled liquid state.

4.2 Case A

Hereafter, we occasionally compare the results with those in the case without the small ice crystal in our previous paper (Nobekawa et al. [18]). For simplicity, we do not add the reference number to each comparison.

4.2.1 Zenith angle

The time change in the z-component of the zenith angle of the segment shows whether or not a part of the segment is affected by the prism face of the ice crystal. This is because the prism faces and the helical axis of the segment were parallel to the z-axis at the initial stage. Figure 7(a)–(c) depict the time change in the z-component of the TT segment, that of the VV segment and that of the SS segment, respectively. The component of the VV segment is found to fluctuate in the range of 0°–6° in Figure 7(b). This is similar to that in the case without the ice crystal.

The component of the SS segment increases within a very short time after $t = 0$ ps as shown in Figure 7(c). Then, the component fluctuates in the range of 15°–20°. Although, the rapid increase and values in the component of the SS segment are different from those of the VV segment, the range width and stable tendency in the component of the SS segment are the same as those of the VV segment.

In contrast with the results mentioned above, the component of the TT segment increases for the period of 125 ps as time proceeds (see Figure 7(a)). Then, the average value of the component reaches approximately 14°. This value is higher than that in the case without the ice crystal. Thus, the motion of the TT segment is affected by the ice crystal.

4.2.2 Relative displacement of sites

In order to investigate the difference in the motion of the segments in more detail, relative displacement from an initial position of each site is examined. The coordinate origin is at the centre of the ice crystal. Figures 8–10 exhibit the results of the oxygen sites of the TT segment, those of the methyl sites of the VV segment, and those of the oxygen sites of the SS segment, respectively. A negative value of the relative displacement in the x- or y-direction indicates the approach of a site to the prism face.

It is found from Figure 9 that the relative displacements of three sites in the VV segment fluctuate around their time-averaged values. These values are positive in the directions except for that of the methyl site of Val35. Particularly, the oxygen site of Asn27 maintains high positive values in the x-direction, while it maintains slightly positive values in the y-direction. This shows that Asn27 is kept away from the ice face. Since, the valine residues have two methyl sites and no hydroxyl site, the possibility is very low for a hydrogen bond occurring between these residues and water molecules. Consequently, the water molecules near the residues can move easily, and thus do not affect the motion of the residues.

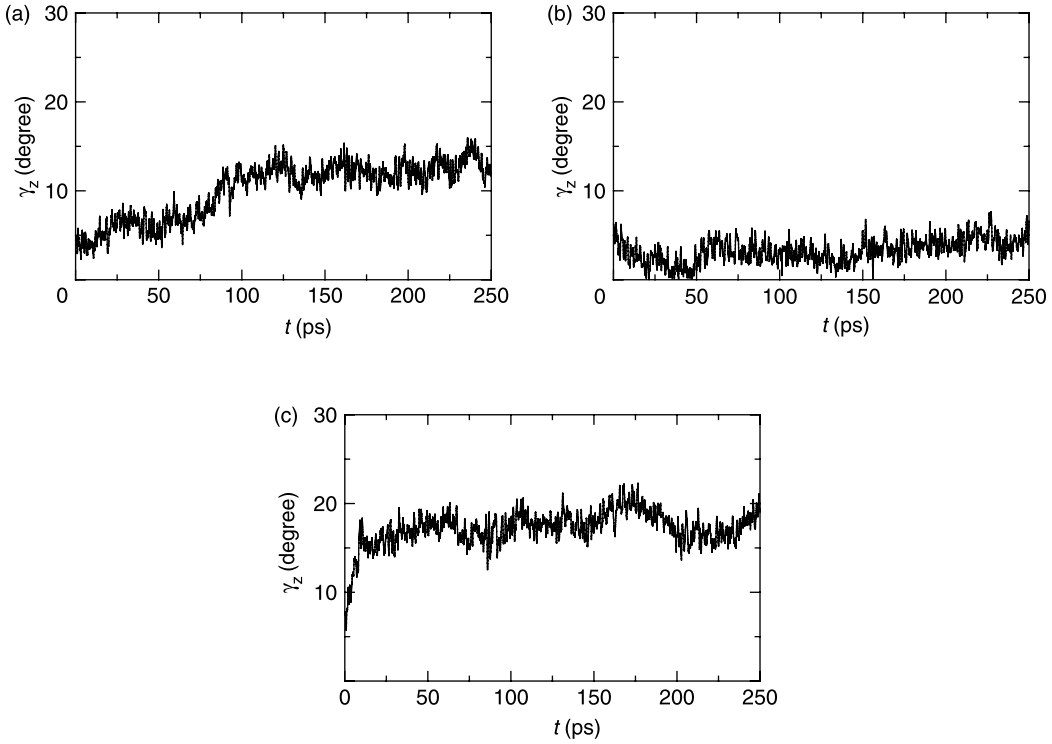

Figure 7. Time changes in the *z*-component of zenith angle: (a) TT segment, (b) VV segment and (c) SS segment.

The relative displacement of the oxygen site of Asn27 in the SS segment reaches high positive values in the *x*- and *y*-directions, as shown in Figure 10. The relative displacement of the oxygen site of Ser35 reaches higher positive values in the *x*-direction than the values of Asn27, while it fluctuates at around 0 nm in the *y*-direction. This result shows that Ser35 moves away from the ice face. Since the serine residues have three hydrogen sites, one oxygen site and no methyl site, the water molecules are attracted by these hydrophilic sites. The duration of the hydrogen bond between these sites and water molecules is very short. Thus, the water molecules near Ser35 can move much easier than those near the other residues. The motion of Ser35 is the result of interaction between the hydrophilic sites and water molecules with such high mobility.

The relative displacement of the oxygen site of Ser24 reaches negative values in the *x*-direction, while it reaches positive values in the *y*-direction. Consequently, Ser24 only slightly approaches the ice face. The noticeable increase in the displacement of the oxygen site in Ser35 in the period of 0–10 ps and the noticeable decrease in the displacement of the oxygen site in Ser24 correspond to the rapid change in the zenith angle as shown in Figure 9.

On the other hand, it is found from Figure 8 that the relative displacement of the oxygen site of Thr24 in the *x*-direction decreases as time proceeds from −50

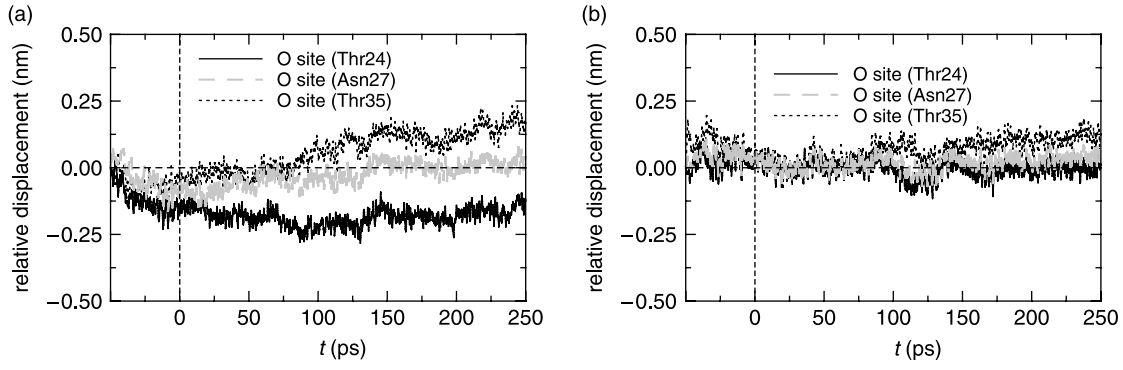

Figure 8. Relative displacement of oxygen sites in TT segment: (a) *x*-direction, (b) *y*-direction.

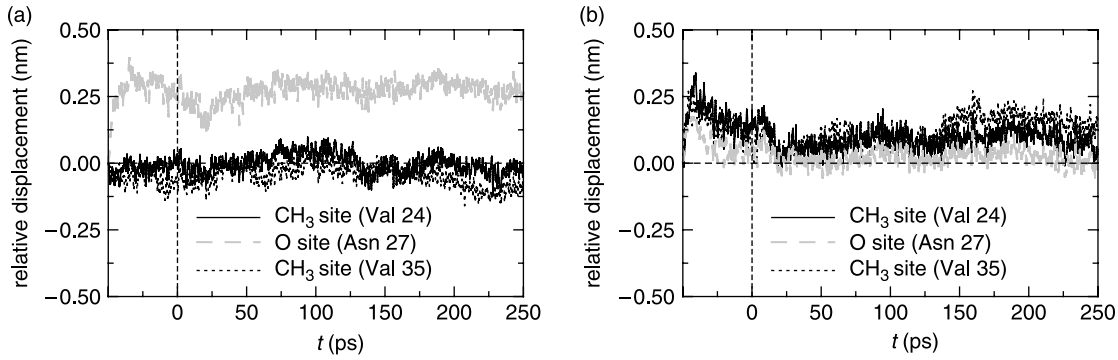

Figure 9. Relative displacement of oxygen site and methyl sites in VV segment: (a) *x*-direction, (b) *y*-direction.

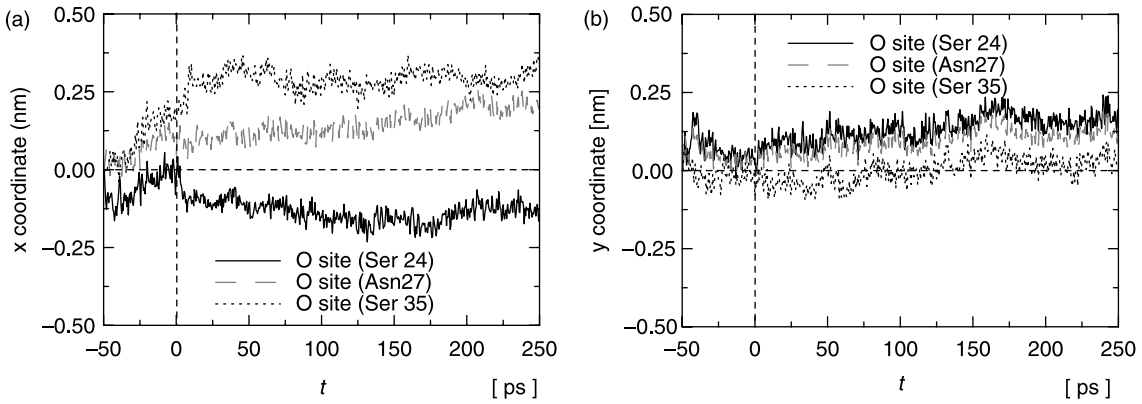

Figure 10. Relative displacement of oxygen sites in SS segment: (a) *x*-direction, (b) *y*-direction.

to 125 ps, while the relative displacements of the oxygen sites of Asn27 and Thr35 in the *x*-direction increase as time proceeds from −25 to 125 ps. The relative displacements of the oxygen sites in the *y*-direction do not change remarkably in the period. Thus, Thr24 in the segment approaches the prism face of the ice crystal, while Thr35 recedes from the face. This difference in the motion between the two threonine residues is due to Asn27 near Thr24.

We made Ser24 by replacing the methyl site of Thr24 with a hydrogen atom. The hydrogen atom of Thr24, which faces the two hydrogen atoms of Asn27 (H_{N1} and H_{N2}), remains in Ser24. Therefore, the hydrogen bond between the oxygen atoms of two water molecules and the three hydrogen atoms in Ser24 and Asn27 is as high as the possibility of the hydrogen bond between the oxygen atoms of two water molecules and the three hydrogen atoms in Thr24 and Asn27 discussed in our previous paper. This is the reason for the similarity of the location of Ser24 to the location of Thr24.

4.2.3 Hydrogen bond to oxygen sites or hydrogen sites

We examine the time changes in the HBCF concerning the oxygen site of the hydroxyl group of Thr24. Figure 11 depicts the time changes in the HBCF for the three periods. The hydrogen bond between the oxygen site of the hydroxyl group and the hydrogen atom of any water molecule in the ice crystal is excluded from the calculation in order to discuss only the interaction of the sites with the water molecule in the liquid phase. It is confirmed from Figure 11 that the HBCF maintains higher values as the hydroxyl group approaches the prism face of the ice crystal. Thus, it can be considered that the

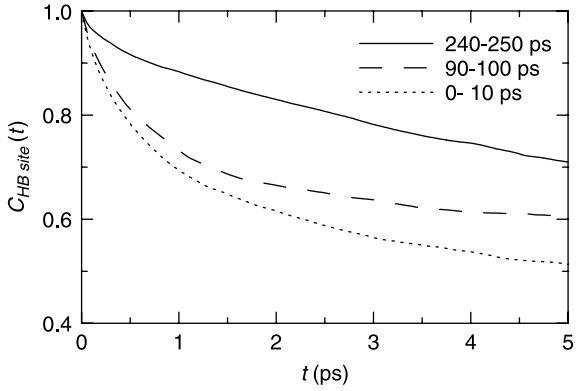

Figure 11. HBCFs.

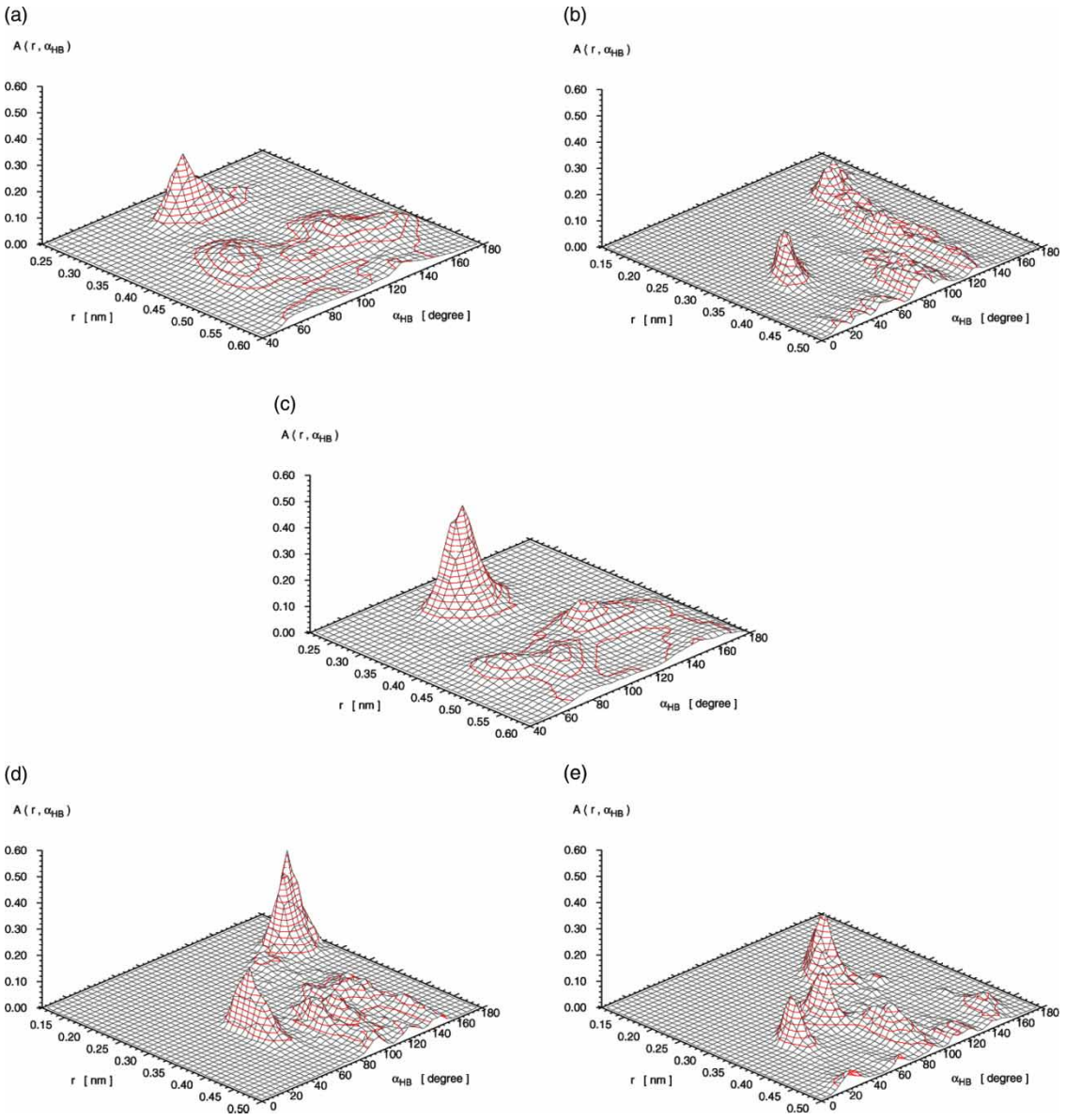

Figure 12. ADFs of water molecules concerning the oxygen site of the hydroxyl group in threonine residue (Thr24): (a) oxygen site of Thr24 ($O\cdots O_w—H_{wfar}$), (b) hydrogen site of Thr24 ($O—H\cdots O_w$), (c) oxygen site of Asn27 ($O\cdots O_w—H_{wfar}$), (d) hydrogen site (H_{N1}) of Asn27 ($N—H_{N1}\cdots O_w$) and (e) hydrogen site (H_{N2}) of Asn27 ($N—H_{N2}\cdots O_w$).

clustering of the water molecules around the oxygen site advances.

Next, we examine the ADF of water molecules surrounding the oxygen site. To avoid the error caused by the RDF, which is used as a weighting function for the ADF, even the water molecules in the ice crystal were taken into account. Figure 12(a) and (c) indicate the results of the period of the final 50 ps. A low peak at 90° and a high peak at 130° are seen clearly inside the second hydration shell ($r \leq 0.55$ nm), with respect to the oxygen site of Thr24 (see Figure 12(a)). These peaks are also seen inside the shell, with respect to the oxygen site of Asn27 (see Figure 12(c)). However, these peaks are not seen in the case without the ice crystal at 300 K (see Figure 9(a) and (c) in our previous paper), nor is the peak at 130° seen in the case without the ice crystal at 230 K (see Figure 10(a) and (c) in our previous paper). Thus, the peaks at 130° are peculiar to the ADF in the present case. It can be concluded that the water molecules bind to the oxygen site of the hydroxyl group by the hydrogen bond and that they are coordinated in a similar way to the water molecules inside the ice crystal.

The ADF of water molecules surrounding the hydrogen site of Thr24 shown in Figure 12(b) is similar to that in the case without the ice crystal at 230 K (see Figure 10(b), in our previous paper [18]) except for

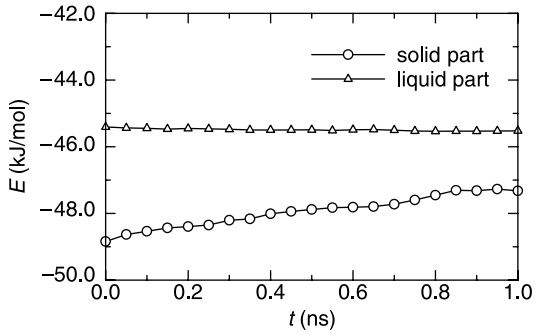

Figure 13. Time changes in potential energy.

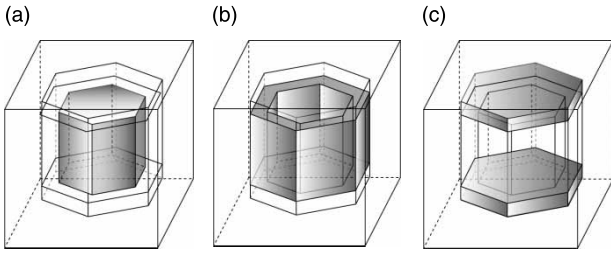

Figure 14. Three regions in the ice crystal: (a) central region, (b) prism face region, (c) basal face region.

the fact that the peak at $r = 0.21$ nm and $\alpha_{HB} = 156°$ becomes low in Figure 12(b). The ADFs of hydrogen sites of Asn27 shown in Figure 12(d) and (e) are similar to those respectively, in the case without the ice crystal at 230 K (see Figure 10(d) and (e), in our previous paper [18]) except for the fact that a new peak appears at $r = 0.30$ nm and $\alpha_{HB} = 84°$ in Figure 12(e). These results suggest that the hydrogen sites in the hydroxyl group of Asn27 and the threonine residues enhance the hydrogen bond between the oxygen atoms of some water molecules and these hydrogen sites, as is mentioned in our previous paper. Furthermore, these water molecules are located in the vicinity of the ice crystal face because the distance between the oxygen site in the hydroxyl group of Thr24 and the ice face is shorter than 0.3 nm, which is estimated from the relative displacement after 100 ps shown in Figure 8 and the size of the ice crystal. Judging from this distance, the possibility of the hydrogen bond existing between the hydrogen atoms of these water molecules and the oxygen atoms of the water molecules in the ice crystal is very high. In this case, the motion of the water molecules is restrained due to the hydrogen bonds by both the ice crystal and the two residues. This shows that Thr24 and Asn27 are not necessarily adsorbed to the ice crystal but are located stably in the vicinity of the ice crystal face.

4.3 Case B

4.3.1 Duration of ice crystal

Figure 13 indicates the time changes in the potential energies of the liquid and solid phases in the case without any segment. The absolute value of the energy in the solid phase decreases, while that in the liquid phase increases as time proceeds. This decrease in the potential energy of the solid phase shows a gradual melting of the ice crystal.

In order to examine this melting in detail, we divide the ice crystal into three regions (central region, prism face region and basal face region, as shown in Figure 14) and investigate the MSD of water molecules in these regions. Figure 15(a) shows the MSD for the period of 0–50 ps after the beginning of the calculation. The MSD of water molecules in the basal face region maintains higher values than that in the other regions. This indicates that the water molecules on the basal faces diffuse more than those on the prism faces. This is reasonable because the solid angle of the water molecules on the edge of the basal face is much wider than that of the water molecules on the prism faces, and thus the water molecules on the edge receive more influence of the water molecule in the liquid phase than any other molecules in the ice crystal.

Following this, we can assume that the value of the MSD of the water molecules in the basal face region at a time is a threshold, and consider that the ice crystal is maintained as long as the MSD of the water molecules in

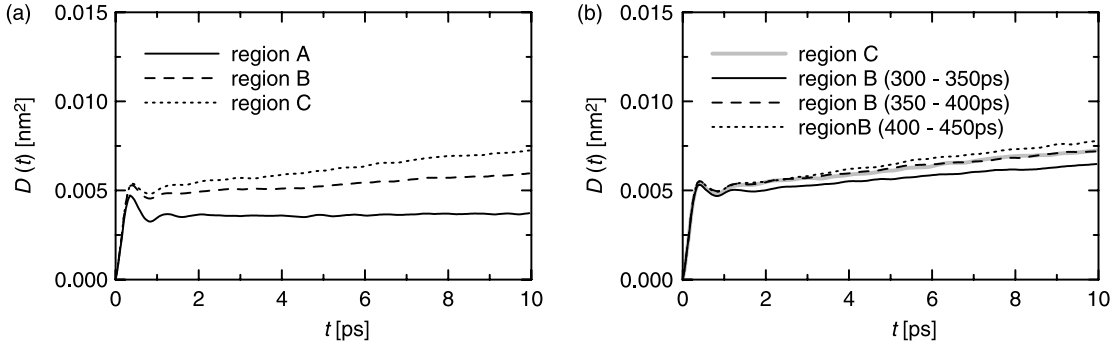

Figure 15. MSDs of water molecules inside the large ice crystal: (a) in the period of 0–50 ps, (b) in three periods.

the prism face region does not exceed the threshold. In Figure 15(b), we find that the MSD exceeds the threshold for the period of 400–450 ps. Thus, we conclude that the results until 400 ps are trustworthy.

4.3.2 *Zenith angle*

Figure 16 shows the time changes in the *x*-, *y*- and *z*-component of the zenith angle of segments axes. The segments are numbered from 1 to 5 counter-clockwise when they are viewed in the opposite direction of the *z*-axis, as in Figure 2(b). Figure 16 shows that each segment fluctuates around the initial position. The time-averaged values of the fluctuating angles depend on the components and segment locations. However, the amplitude of the fluctuation of each segment is not so different from that in the case without the ice crystal.

4.3.3 *MSD, CFR and HBCF of water molecules*

In order to extract the effect of five segments, we compare the statistics of water molecules in a region including the segments with those in another region without the segments. Figure 17 shows these regions, which are symmetrically positioned with respect to the

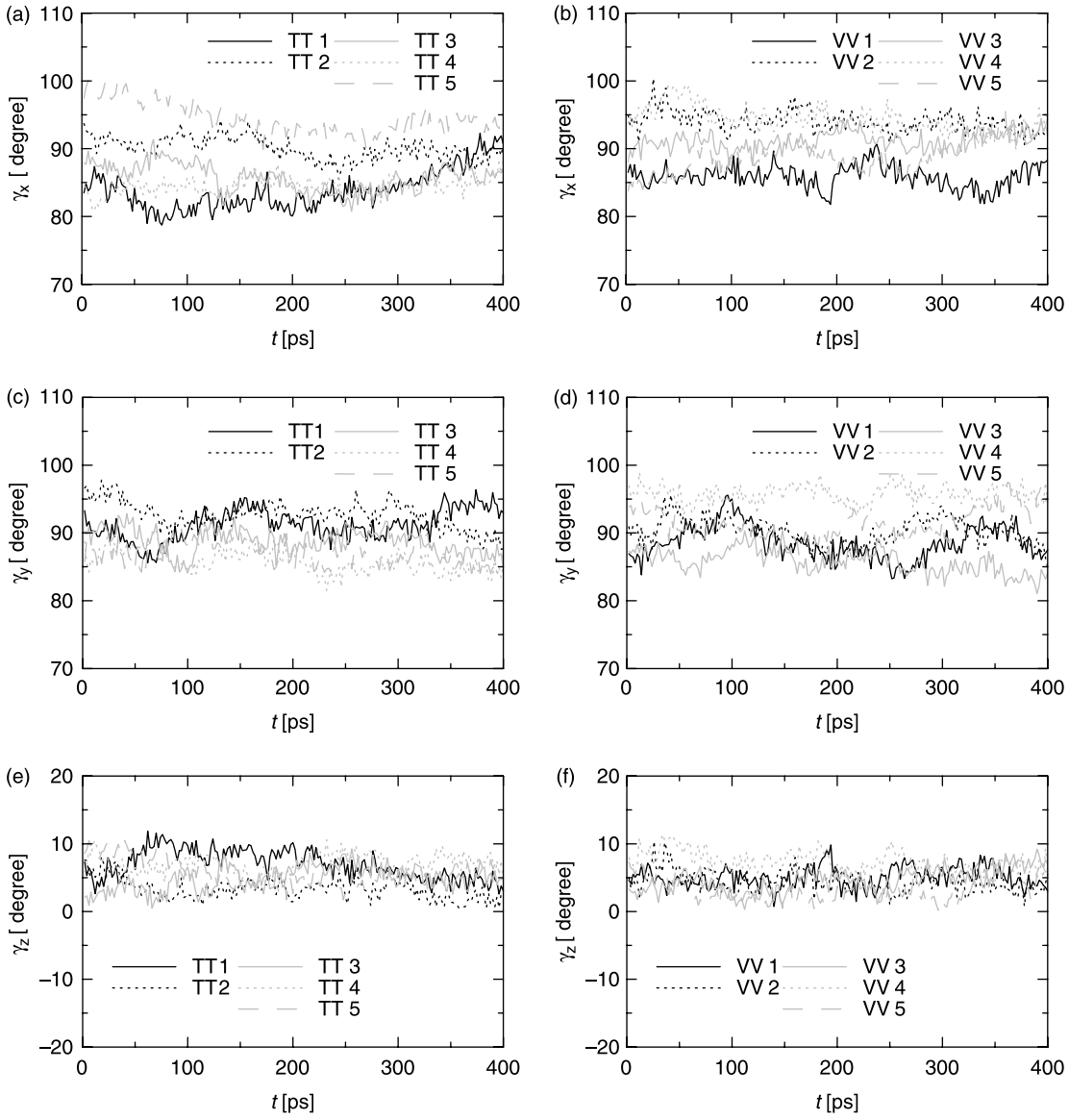

Figure 16. Time changes in the components of zenith angles of segments: (a) *x*-components of TT segments, (b) *x*-components of VV segments, (c) *y*-components of TT segments, (d) *y*-components of VV segments, (e) *z*-components of TT segments and (f) *z*-components of VV segments.

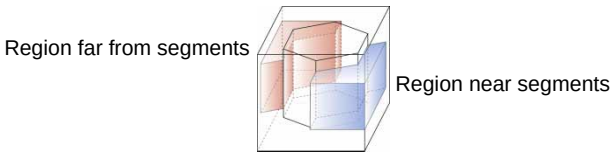

Figure 17. Region near segments and region far from segments.

c-axis of ice crystal. Hereafter, the region including the segments is called 'region near the segments' and the other region is called 'region far from the segments'.

Figure 18 compares the MSD of the water molecules in the region near the segments with that in the region far from the segments. The MSD was obtained from the moving averages in the periods of 0–10, 0.25–10.25, . . . , 390–400 ps. The initial instants for these moving averages are indicated as $t = 0$ ps for simplicity. The MSD of the water molecules in the region near the segments is lower than that in the region far from the segments. Thus, the diffusion of water molecules in the liquid phase is restrained by the segments.

Figure 19 indicates the CFR of the water molecules in the region near the segments and that in the region far from the segments. The CFR is obtained from the moving averages. This is the same as that of the MSD mentioned above. The CFR of the water molecules in the region near the segments is higher than that in the region far from the segments. The fluctuation of rotational motion of water molecules is attenuated by the segments.

Figure 20 compares the HBCF of the water molecules in the region near the segments with that in the region far from the segments. The HBCF is obtained from the moving averages. This is the same as that of the MSD mentioned above. The HBCF of the water molecules in the region near the segments is higher than that in the region far from the segments. Thus, the clusters of water molecules are maintained by the existence of the segments.

Since the mobility of water molecules decreases with temperature, the effect of the initial condition on the statistics of the motion of water molecules for a predetermined period becomes remarkable as the temperature becomes low. Thus, the statistics in the case of supercooled water with the ice crystal and the segments cannot be directly compared with those in the case of water with the segment at 300 K. Nevertheless, the following fact is obtained from the results mentioned above and the results in the case without the ice crystal: the inhibition action against the motion of water molecules by the VV segments is more remarkable than that by the TT segments. This suggests that the water molecules around the methyl sites gathered due to the hydrophobic hydration have more influence on the other water molecules, compared with the influence of water molecules around the hydrogen sites gathered due to the hydrogen bond.

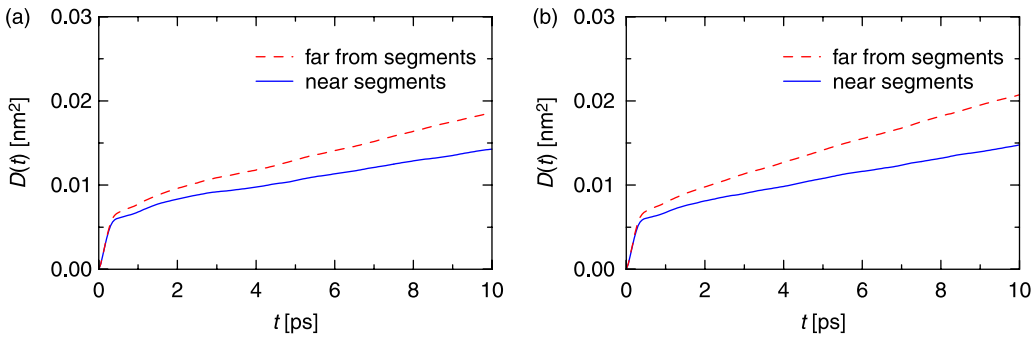

Figure 18. MSDs: (a) in the case with TT segments, (b) in the case with VV segments.

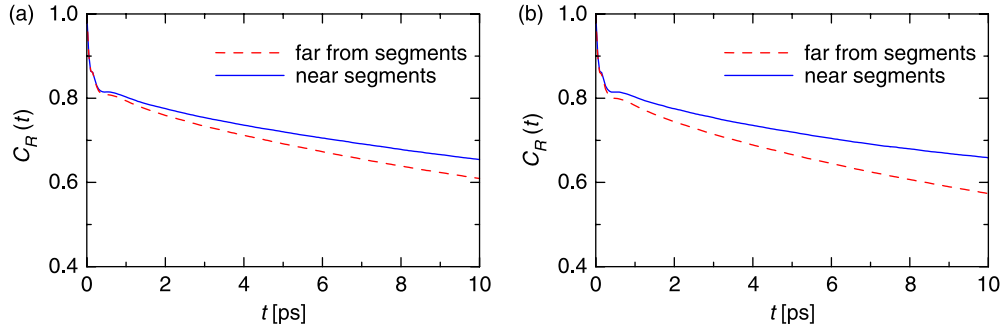

Figure 19. Correlation function of rotation: (a) in the case with TT segments, (b) in the case with VV segments.

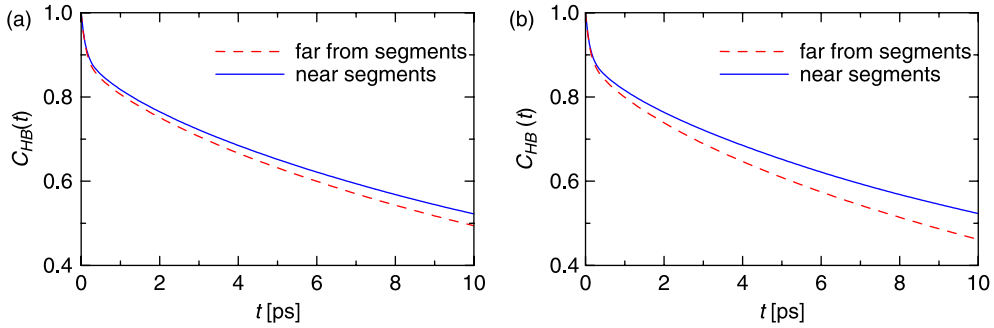

Figure 20. HBCF (a) in the case with TT segments, (b) in the case with VV segments.

4.3.4 *ADF and dihedral angle of water molecules*

Figure 21(a) displays the ADF of water molecules surrounding the oxygen sites of Thr24 in the five TT segments, while Figure 21(c) displays the ADF of water molecules surrounding the oxygen sites of Asn27 in the segments. These figures are similar to Figure 11(a) and (c) in Case A, respectively. However, it is noted that the heights of peaks are clearly different.

Figure 21(b) shows the ADF of water molecules near the hydrogen sites of Thr24 in the five TT segments. Figure 21(d) shows the ADF of water molecules near the hydrogen site (H_{N1}) of Asn27 in the segments. Figure 21(e) shows the ADF of water molecules near the hydrogen site (H_{N2}) of Asn27 in the segments. These figures are also similar to Figure 11(b)–(e) in Case A, respectively. Note that similar ADFs are also obtained for the water molecules near the oxygen site and hydrogen sites of Asn27 in the VV segments (figure omitted). Thus, the hydrogen bond does exist around the site of the segments.

Figure 22(a) shows the DADF concerning the methyl sites of alanine residues in the TT segments. Figure 22(b) indicates the DADF concerning the methyl sites of alanine residues in the VV segments. These distributions are similar to that in the case without the ice crystal. It is concluded that the water molecules around the hydrophobic sites of the five segments gathered due to the hydrophobic hydration exert an influence on the other surrounding water molecules.

The DADF concerning the methyl sites of the threonine residues in the TT segments is shown in Figure 23(a). The DADF concerning the methyl sites of the valine residues in the VV segments is indicated in Figure 23(b). The distributions of the angles are also similar to those of the angles concerning the alanine residues. It is striking that not only the water molecules around the alanine residues gathered due to the hydrophobic hydration but also those around the methyl sites of threonine residues due to hydrophobic hydration contribute to the antifreeze effect of the HPLC6.

5. Conclusion

A molecular dynamics simulation was carried out for the mixture of supercooled water, a hexagonal ice crystal and one rigid TT α-helical segment, which simulated the part of antifreeze protein type I. The VV segment, in which the two threonine residues of the TT segment were replaced with valine residues, and the SS segment, in which the two threonine residues were replaced with serine residues, were also used. Furthermore, the mixture of supercooled water, a large ice crystal and five TT segments was dealt with. The main conclusions obtained are as follows:

(1) The MSD, the CFR, the ADF, the DADF and the HBCF are effective for analysing the interaction of water molecules and the segments.
(2) The threonine residue close to the asparagine residue of the TT segment approaches the prism face of the hexagonal ice crystal. This is possibly because of the hydrogen bond between the hydrogen sites in the hydroxyl group of these residues and the oxygen atoms of some water molecules, and the hydrogen bond between the hydrogen atoms of these water molecules and the oxygen atoms of the water molecules in the ice crystal.
(3) The VV segment does not approach the prism face. This is because of the lack of hydrophilic sites, which is effective for the hydrogen bond to the water molecules between the model and ice face.
(4) Ser24 in the SS segment approaches the ice face only slightly. One of the three hydrogen sites of Ser24 is the same as that of Thr24, which faces the two hydrogen atoms of Asn27. Thus, the possibility of the hydrogen bond occurring among the hydrogen sites in Ser24 and Asn27 and water molecules is similar to the possibility of the hydrogen bond occurring among the hydrogen sites in Thr24 and Asn27 and water molecules mentioned in (2). On the other hand, Ser35 moves

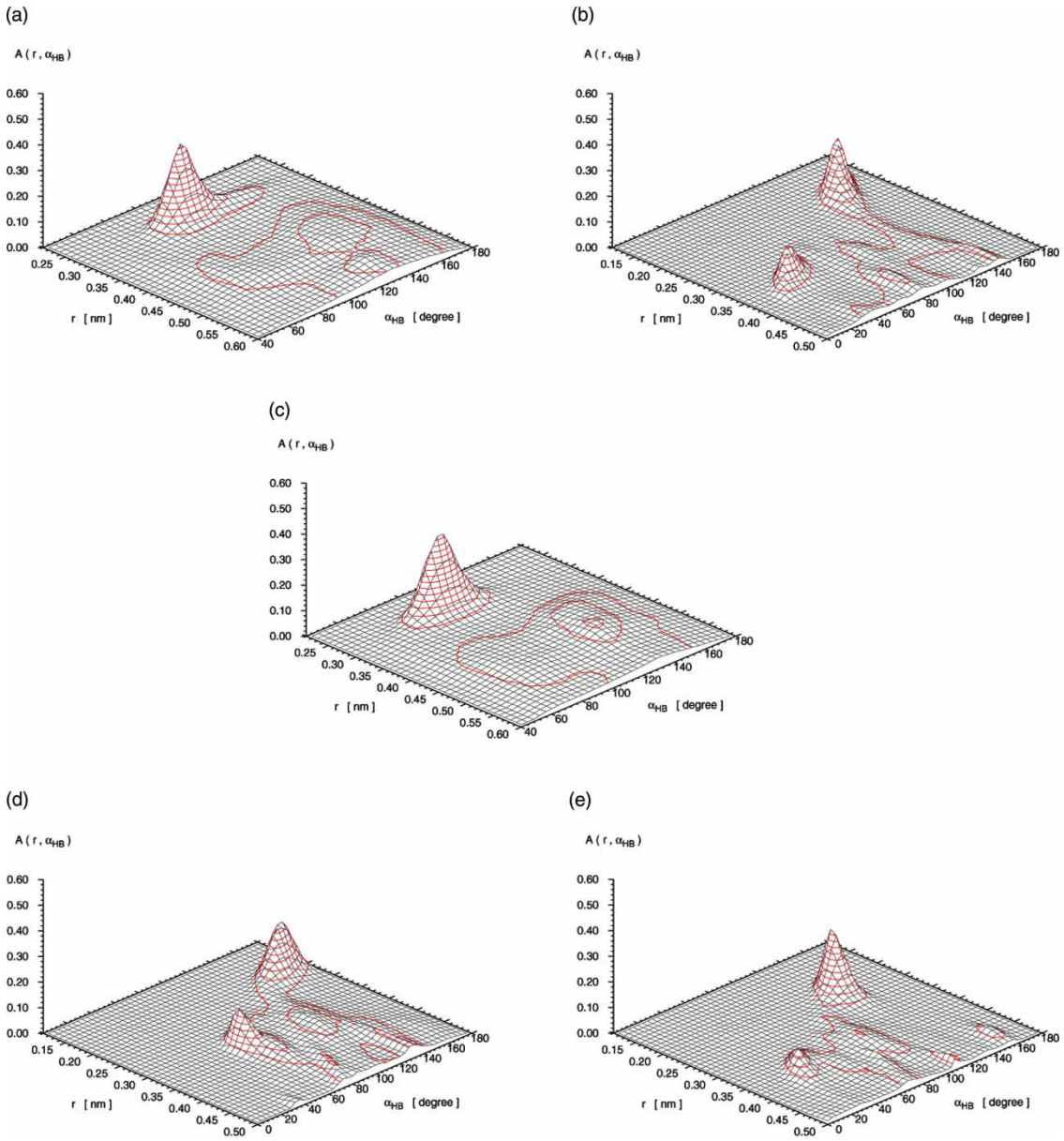

Figure 21. ADFs of sites of TT segments: (a) oxygen site of Thr24 ($O\cdots O_w—H_{w\,far}$), (b) hydrogen site of Thr24 ($O—H\cdots O_w$), (c) oxygen site of Asn27 ($O\cdots O_w—H_{w\,far}$), (d) hydrogen site (H_{N1}) of Asn27 ($N—H_{N1}\cdots O_w$) and (e) hydrogen site (H_{N2}) of Asn27 ($N—H_{N2}\cdots O_w$).

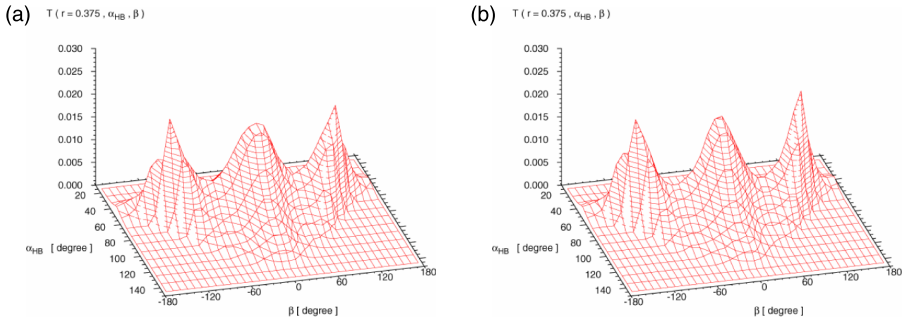

Figure 22. DADFs of water molecules near methyl sites of alanine residues: (a) in the case with TT segments, (b) in the case with VV segments.

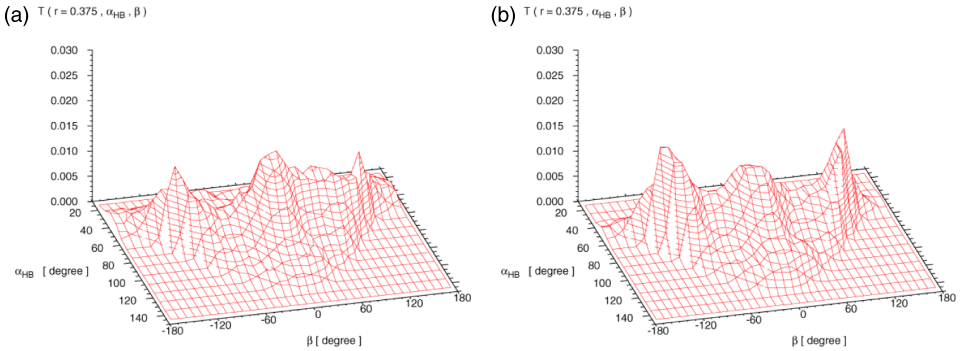

Figure 23. DADFs of water molecules near methyl sites: (a) Thr24 and Thr35, (b) Val24 and Val35.

away from the face. This is due to the four hydrophilic sites, which attract water molecules around the sites. This is consistent with the experimental results obtained by Zhang and Laursen.

(5) The gathering of water molecules caused by the hydrophobic hydration occurs not only around the alanine residues but also around the methyl sites of the threonine residues. The gathered water molecules have an influence on the other water molecules near the residues.

(6) The motions of five TT segments closely located side by side, which simulate an aggregated state of segments, are not remarkable compared with the motion of a single segment.

Acknowledgments

This study was partially supported by the Ministry of Education, Culture, Sports, Science and Technology of Japan through the Grant-in-Aid for Exploratory Research (No. 16656071) and the Grant-in-Aid for Scientific Research (C) (No. 19560206). The authors acknowledge Mr H. Taniguchi for his assistance of supplemental computation. The authors also acknowledge Professor H. Urakawa at Department of Chemistry and Materials Technology, Kyoto Institute of Technology, for his kind checking of the manuscript.

Note

1. Tel.: +81-75-724-7327. Fax: +81-75-724-7300. E-mail: bluestar0917t@m3.dion.ne.jp

References

[1] B. Li and D-W. Sun, *Novel methods for rapid freezing and thawing of foods – a review*, J. Food Eng. 54 (2001), p. 175.

[2] G.L. Fletcher, S.V. Goddard, and Y. Wu, *Antifreeze proteins and their genes: From basic research to business opportunity*, Chem. Tech. 30(6) (1999), p. 17.

[3] G. Amir, B. Rubinsky, S.Y. Basheer, L. Horowitz, L. Jonathan, M.S. Feinberg, A.K. Smolinsky, and L. Lavee, *Improved viability and reduced apoptosis in sub-zero 21-hour preservation of transplanted rat hearts using anti-freeze proteins*, J. Heart Lung Transplant. 24 (2005), p. 1915.

[4] D.S.C. Yang, M. Sax, A. Chakrabatty, and C.L. Hew, *Crystal structure of an antifreeze polypeptide and its mechanistic implications*, Nature 333 (1988), p. 232.

[5] C.A. Knight, C.C. Cheng, and A.L. DeVries, *Adsorption of alpha-helical antifreeze peptides on specific ice crystal surface planes*, Biophys. J. 59 (1991), p. 409.

[6] Y. Yeh and R.E. Feeney, *Antifreeze proteins: Structures and mechanisms of function*, Chem. Rev. 96 (1996), p. 601.

[7] H. Chao, M.E. Houston Jr., R.S. Hodges, C.M. Kay, B.D. Sykes, M.C. Loewen, P.L. Davies, and F.D. Sönnichsen, *A diminished role for hydrogen bonds in antifreeze protein binding to ice*, Biochemistry 36 (1997), p. 14652.

[8] W. Zhang and R.A. Laursen, *Structure–function relationships in a type I antifreeze polypeptide*, J. Biol. Chem. 273 (1998), p. 34806.

[9] A.D.G. Haymet, L.G. Ward, and M.M. Harding, *Winter flounder 'antifreeze' proteins: Synthesis and ice growth inhibition of analogues that probe the relative importance of hydrophobic and hydrogen-bonding interactions*, J. Am. Chem. Soc. 121 (1999), p. 941.

[10] M.C. Loewen, H. Chao, M.E. Houston, J. Baardsnes, R. Hodges, C.M. Kay, B.D. Sykes, F.D. Sönningen, and P.L. Davies, *Alternative roles for putative ice-binding residues in type I antifreeze protein*, Biochemistry 38 (1999), p. 4743.

[11] A. Jorov, B.S. Zhorov, and D.S.C. Yang, *Theoretical study of interaction of winter flounder antifreeze protein with ice*, Protein Sci. 13 (2004), p. 1537.

[12] A. Cheng and M. Merz, *Ice-binding mechanism of winter flounder antifreeze proteins*, Biophys. J. 73 (1997), p. 2851.

[13] P. Dalal, J. Krickelbein, A.D.G. Haymet, F.D. Sönnichsen, and J. Madura, *Hydrogen bond analysis of type 1 antifreeze protein in water and the ice/water interface*, PhysChemComm 7 (2001), p. 1.

[14] A. Wierzbicki, P. Dala, T.E. Cheatham III, J.E. Knickelbein, A.D.J. Haymet, and J.D. Madura, *Antifreeze proteins at the ice/water interface: Three calculated discriminating properties for orientation of type I proteins*, Biophys. J. 93 (2007), p. 1442.

[15] C. Yang and K.A. Sharp, *Hydrophobic tendency of polar group hydration as a major force in type I antifreeze protein recognition*, Proteins: Struct. Funct. Bioinform. 59 (2005), p. 266.

[16] A.D.G. Haymet, L.G. Ward, M.M. Harding, and C.A. Knight, *Valine substituted winter flounder 'antifreeze': Preservation of ice growth hysteresis*, FEBS Lett. 430 (1998), p. 301.

[17] R. Coger, B. Rubinsky, and G. Fletcher, *Microscopic pattern of ice crystal growth in the presence of thermal hysteresis proteins*, (Trans. Am. Soc. Mech. Eng.) J. Offshore Mech. Arotic Eng. 116 (1994), p. 173.

[18] T. Nobekawa, H. Taniguchi, and Y. Hagiwara, *Interaction between a twelve-residue segment of antifreeze protein type I, or its mutants, and water molecules*, Mol. Simul. 34 (2008), p. 309.

[19] C.W. Gear, *Numerical Initial Value Problems in Ordinary Differential Equations*, Prentice-Hall, Englewood Cliffs, 1971.
[20] K. Iwasaki and Y. Hagiwara, *Inhibition of ice nucleus growth in water by alanine dipeptide*, Mol. Simul. 30 (2004), p. 487.
[21] W.J. Jorgensen, J. Chandrasekhar, J.D. Madura, R.W. Impey, and M.L. Klein, *Comparison of simple potential functions for simulating liquid water*, J. Chem. Phys. 79 (1983), p. 926.
[22] M. Matsumoto, S. Saito, and I. Ohmine, *Molecular dynamics simulation of the ice nucleation and growth process leading to water freezing*, Nature 416 (2002), p. 409.
[23] H. Nada, J.P. van der Eerden, and Y. Furukawa, *A clear observation of crystal growth of ice from water in a molecular dynamics simulation with a six-site potential model of H_2O*, J. Crystal Growth 266 (2004), p. 297.
[24] L. Verlet, *Computer 'experiments' on classical fluids. II. Equilibrium correlation functions*, Phys. Rev. 165 (1968), p. 201.
[25] D. Frenkel and B. Smit, *Understanding Molecular Simulation*, Academic Press, San Diego, 1996.
[26] J.P. Ryckart, G. Ciccotti, and H.J.C. Berendsen, *Numerical integration of the Cartesian equations of motion of a system with constraints: Molecular dynamics of* n*-alkanes*, J. Comput. Phys. 23 (1977), p. 327.
[27] W.J. Jorgensen and J. Tirado-Rives, *The OPLS potential functions for proteins: Energy minimisations for crystals of cyclic peptides and crambin*, J. Am. Chem. Soc. 110 (1988), p. 1657.
[28] A.W. Reach, *Molecular Modelling – Principles and Applications*, 2nd ed., Pearson Education Ltd 1996.
[29] D.H. Nguyen, M.E. Colvin, Y. Yeh, R.E. Feeney, and W.H. Fink, *Intermolecular interaction studies of winter flounder antifreeze protein reveal the existence of thermally accessible binding state*, Biopolymers 75 (2004), p. 109.
[30] M.P. Allen and D.J. Tildesley, *Computer Simulation of Liquid*, Oxford Science, Oxford, 1987.
[31] M. Umemura, T. Nakagawa, S. Hayashi, H. Urakawa, and K. Kajiwara, *Structure of water molecules in aqueous maltose and cellobiose solutions using molecular dynamics simulation. II. Dynamics*, J. Mol. Struct. (Theochem) 636 (2003), p. 215.